Inhibiting migration of endothelial-derived mesenchymal cells using a nanoparticle-based photothermal treatment impedes atherosclerosis and cancer progression

Xin Luo [a, b], Xiao Yu [a, b], Vanessa Kee [a, b], Steve J. Smith [a, b], Congzhou Wang [a, b] *

[a] Nanoscience and Biomedical Engineering, South Dakota School of Mines and Technology, 501 E St Joseph Street, Rapid City, South Dakota, USA, 57701

[b] BioSystems Networks & Translational Research (BioSNTR), 501 E St Joseph Street, Rapid City, South Dakota, USA, 57701

* Please direct all correspondence to: congzhou.wang@sdsmt.edu

Abstract: The migration and invasion of endothelial-derived mesenchymal cells (EMCs) play a crucial role in both atherosclerotic plaque formation and cancer metastasis. However, current strategies aimed at suppressing EMC formation often suffer from poor specificity and undesirable side effects, and few efforts have directly targeted the migratory and invasive behavior of EMCs. In this study, we present a nanoparticle-based strategy to specifically inhibit EMC migration and invasion using cadherin-2 targeted melanin nanoparticles in combination with mild photothermal treatment. Cell migration and invasion assays demonstrate that the synergistic effect of nanoparticle uptake and photothermal treatment effectively impedes EMC motility. Atomic force and super resolution microscopy indicate that this inhibition is associated with disruption of the actin cytoskeleton and consequent morphological alterations. Furthermore, Western blot analyses elucidate the underlying molecular mechanism, showing that cadherin-2 dependent RhoA activation is downregulated by the combined nanoparticle and photothermal treatment, leading to cytoskeletal disorganization. Overall, these in vitro findings serve as a proof-of-concept study for a potential alternative or complementary strategy to attenuate atherosclerotic plaque development and cancer metastasis by targeting the migration and invasion of EMCs from a mechanistic perspective.

Keywords: Endothelial-derived mesenchymal cells; Migration; Photothermal nanoparticles; Atherosclerosis; Cancer.

Introduction

Endothelial-derived mesenchymal cells (EMCs) refer to cells originating from endothelium that have experienced a cellular transformation process, namely, endothelial-to-mesenchymal transition (EndMT).[1] During this process, resident endothelial cells lining the interior wall of blood vessels lose their endothelial markers and barrier functions, and acquire mesenchymal-type, migratory features, leading to their migration and invasion to underlying tissues.[2-3] Although earlier studies demonstrated that EndMT plays a critical role in the embryonic development, recent evidence suggests that EndMT-produced EMCs are associated with multiple pathologies including atherosclerosis and cancer.[4-5] In the early stage of atherosclerosis, persistent activation of endothelial cells triggers EndMT, wherein migratory EMCs penetrate through the arterial intima, enter the atherosclerosis plaque, and coordinate with other cells to advance plaque formation.[6-7] In the context of cancer, EndMT-produced EMCs are considered as a major source (40%) of cancer-associated fibroblasts (CAFs).[8] As mesenchymal cells, CAFs contribute to tumor progression in several ways including physically pulling cancer cells forward or creating moving-paths for cancer cells through their own migration (i.e., leader-follower dynamics, **Figure 1**).[9-12] Accordingly, EMCs, especially their migration, could serve as a potential therapeutic target for slowing down atherosclerosis and cancer progression at their early stages.

Clinical studies indicated that the proportions of EMCs in atherosclerosis plaques and CAFs in tumors correlate positively with the severity of these diseases.[13-14] Given the primary contribution of EndMT in the production of EMCs and CAFs, current efforts mainly focus on developing molecular drugs to inhibit EndMT of resident endothelial cells, which could reduce the numbers of plaque-associated EMCs and CAFs in tumors.[15] For instance, developing inhibitors against transforming growth factor beta (TGF-β), a classic EndMT-inducing cytokine, has shown effectiveness in alleviating atherosclerosis and cancer by reducing EndMT-produced EMCs.[15-16] However, these TGF-β inhibitors also manifest many side effects owing to the pleiotropic roles of TGF-β signaling in a broad range of cell regulatory pathways and functions, limiting their clinical applications.[17] Another set of inhibitors intended to neutralize pro-inflammatory cytokines such as tumor necrosis factor alpha and interleukin-1 beta have received increased attention, as EndMT

is often considered to be the outcome of chronic inflammation. However, suppressing systemic inflammation could compromise host immunity against bacterial and viral infections.[18-19] Together, these strategies aiming to inhibit EndMT suffer from poor specificity and adverse side effects, and none of these approaches resolve the existing EMCs that have undergone EndMT, especially their migratory/invasive behavior, which significantly contributes to plaque formation and cancer metastasis.

In this work, we show a photothermal nanoparticle-based approach can target and impede the migration of EMCs, namely, cadherin-2 targeted melanin nanoparticles (MelNPs@Cad-2) and their photothermal effect. Our central hypothesis is that MelNPs@Cad-2 will not only specifically target migratory EMCs by recognizing their surface over-expressed cadherin-2,[20-21] but also will modulate the downstream pathway of cadherin-2 which is closely related to the migration behavior of EMCs. Following the nanoparticle uptake, the addition of photothermal treatment v*ia* near-infrared laser irradiation will further disrupt the cadherin-2 pathway and impede the migration of EMCs. By doing so, EMC-led plaque buildup and cancer cell migration can be decreased (**Figure 1**). Unlike traditional photothermal therapy that uses lethal heat (above 50°C) to ablate cancer cells,[22-27] our approach here only needs mild thermal energy (~44°C) to regulate the intracellular signaling related to the migration of EMCs. As such, the disadvantages associated with traditional photothermal therapy, including damage to normal skin (i.e., safety concern), inadequate local temperature to kill cells, and thermal resistance developed by cells (i.e., efficacy concern) can be addressed.[28] To demonstrate the potential applicability of this approach in addressing both atherosclerosis and cancer, we selected two representative endothelial cell models that are well-established for investigating atherosclerosis- and cancer-related EndMT.[29-30] The cell migration/invasion assays suggest the synergistic role of nanoparticle uptake and photothermal treatment in the inhibition of EMC migration/invasion. Further, investigation in cell mechanics using single cell imaging techniques demonstrates the disruption of the actin cytoskeleton of EMCs accounts for the inhibited motility. Finally, the molecular mechanism for disruption of the actin cytoskeleton is elucidated using molecular techniques. Overall, we expect this approach will offer a potential alternative or supplement to hamper the atherosclerosis

plaque formation and cancer metastasis from a new perspective *via* impeding the migration of endothelial-derived mesenchymal cells.

Results and discussion

Preparation and characterization of cadherin-2 targeted melanin nanoparticles

We selected melanin nanoparticles (MelNPs) originating from cuttlefish ink owing to their natural abundance, superior biocompatibility, excellent stability in biofluids, facile surface functionalization, and high efficiency to convert near-infrared light to thermal energy.[31-33] Prior to surface functionalization, MelNPs were purified and collected from cuttlefish ink using a gradient centrifugation method, wherein micrometer-sized particles and large aggregates were separated and discarded through low-speed centrifugation. Following the collection of MelNPs using high-speed centrifugation, the surface of the MelNPs was functionalized with cadherin-2 antibodies through a two-step procedure developed in our group (**Figure 2A**)[34]: (1) The MelNPs were functionalized by a protein layer consisting of Protein A (PA) and Bovine Serum Albumin (BSA) through Michael addition and/or Schiff-base reaction in a mild alkaline environment (pH=8.5); (2) The cadherin-2 antibodies were then conjugated to the surface of MelNPs through the high affinity between Fc region of the antibody and PA. This procedure ensures the Fab domains of the antibody are oriented outward and easy to recognize the cell-surface antigen, while the presence of BSA in the protein layer can be used to regulate antibody density on MelNP surface, avoiding any crowding effect on the antibodies.

Transmission electron microscopy (TEM) revealed size change of MelNPs before and after functionalization of the antibodies. Following functionalization, the average nanoparticle size showed a 2-3 nm increase (from 119.0 to 121.4 nm), suggesting the attachment of antibodies (**Figure 2B-2E**). Dynamic light scattering (DLS) and Zeta potential measurements offered further validations for the successful antibody functionalization of the MelNPs. As shown in **Figure 2F-2G**, the hydrodynamic size of MelNPs gradually increased from 173 nm (bare MelNPs) to 221 nm (MelNPs@PA), and

finally to 263 nm (MelNPs@Cad-2). Meanwhile, the Zeta potential of MelNPs showed a progressive decrease from -31.7 to -40.5 and finally to -41.9 mV, corresponding to bare MelNPs, MelNPs@PA, and MelNPs@Cad-2, respectively. As a non-targeted counterpart, MelNPs coated by neat BSA (i.e., MelNPs@BSA) were also prepared. To test the colloidal stability of MelNPs@Cad-2, they were dispersed in a series of liquid media including H_2O, DPBS, and cell growth medium, and then monitored by UV-vis spectroscopy for 7 days (**Figure 2H**). The minimally changed UV-vis spectra indicated the sustained colloidal stability of MelNPs@Cad-2 in bio-fluids over a 7-day period (**Figure 2I**). Finally, the photothermal property of MelNPs@Cad-2 was evaluated using an 808 nm near-infrared with the intensity at 0.5 W/cm². This power density is close to the laser safety threshold recommended by American National Standards Institute.[28] Within 10 min of laser irradiation, cell growth media containing MelNPs@Cad-2 showed temperature elevations in an irradiation-time and nanoparticle-concentration dependent manner. In particular, the cell medium containing 100 μg/mL of MelNPs@Cad-2 showed a ~7°C increase in temperature after 5 min of laser irradiation (**Figure 2J**). Thus, this moderate photothermal effect, considered as a sub-lethal dose for cells, was chosen for subsequent cellular studies.

Biocompatibility and EMC-targeting ability of MelNPs@Cad-2

To investigate biocompatibility of surface-functionalized MelNPs, human umbilical vein endothelial cells (HUVECs) were selected to be our primary model, since HUVECs from medium-sized vein typically served as a dual model for studying both atherosclerosis in large arteries and cancer metastasis in small capillaries.[35-36] Two standard cytotoxicity assays measuring cell viability (MTT) and membrane damage (LDH) were conducted to assess the endothelial compatibility of 100 μg/mL MelNPs@Cad-2 and MelNPs@BSA. As shown in **Figure 3A**, both versions of nanoparticles, with and without subsequent photothermal treatment, had negligible cytotoxic effects on the HUVECs, suggesting the excellent endothelial compatibility of MelNPs and the mild photothermal treatment. Thus,

these nanoparticle and laser doses were used in the subsequent cell migration experiments reported here.

To evaluate the targeting ability of MelNPs@Cad-2 to EMCs, interleukin-1β (IL-1β), a classic pro-inflammatory cytokine, was selected to activate HUVECs to mesenchymal cells (i.e., EMCs), considering IL-1β is known to induce EndMT and accelerate the progression of both atherosclerosis and cancer.[37-39] After IL-1β activation, cell surface cadherin-2 level dramatically upregulated as demonstrated by the immunofluorescence staining (**Figure 3B-3C, Figure S1**), consistent with previous studies where cadherin-2 is considered as a typical mesenchymal maker for EMCs.[20-21] It was also observed that HUVECs after activation acquired a mesenchymal-like, elongated morphology with an increased cell aspect ratio (**Figure S2**), another hallmark of EndMT-produced EMCs.[40] Next, the non-activated (normal) and activated HUVECs were incubated with MelNPs@Cad-2 and MelNPs@BSA for 12 h and quantified for cellular uptake of nanoparticles based on gray-scale image analysis (**Figure 3D-3E, Figure S3**). In comparison to non-activated (normal, G1) HUVECs, IL-1β activated HUVECs (G4) exhibited a multi-fold increase in the uptake of MelNPs@Cad-2, which could be attributed to the specific binding between MelNPs@Cad-2 and cadherin-2 on the surface of activated HUVECs. The internalized MelNPs@Cad-2 by activated HUVECs were predominantly localized within lysosomes, as shown by the high-degree of co-localization between Lysotrackers (red) and nanoparticles (black) in gray-scale images. In contrast, the activated HUVECs had only modest uptake of non-targeted MelNPs@BSA (G3) and MelNPs@Cad-2 if cells were pre-treated with free cadherin-2 antibodies (i.e., a competition assay, G2), further substantiating the EMC-targeting ability of MelNPs@Cad-2. Collectively, these findings validate the excellent endothelial compatibility of MelNPs@Cad-2 and demonstrate their strong targeting capability toward activated HUVECs (i.e., EMCs).

Anti-migration/invasion effects of MelNPs@Cad-2 and photothermal treatment

Next, we investigated the effects of MelNPs and mild photothermal treatment on the migration and invasion of HUVECs. In the 2D migration assay, the cell migration was

quantified *via* creating a gap on a confluent cell monolayer and measuring the gap closure % in a fixed time frame (9 hours here). As presented in **Figure 4A-4B** and **Figure S4**, activated HUVECs showed significantly enhanced migration ability (100% gap closure) compared to non-activated HUVECs (50% gap closure), confirming the strong migration behavior of EMCs.[4, 41] Treating activated HUVECs using nontargeted MelNPs@BSA and MelNPs@BSA with laser irradiation led to minimal (78% gap closure) and modest (42% gap closure) inhibitory effects on cell migration. Meanwhile, MelNPs@Cad-2 and MelNPs@Cad-2 with laser treatment resulted in a modest (40% gap closure) and a robust (15% gap closure) inhibitory effect on cell migration, respectively. Notably, the combination of MelNPs@Cad-2 and laser treatment almost completely stopped the migration of activated HUVECs. Similar 2D migration results can be obtained in the presence of mitomycin C in order to eliminate the cell proliferation as a confounding factor (**Figure S5**). The results from the 2D migration assays were further confirmed by 3D invasion assays (**Figure 4C-4D**, **Figure S6**), where MelNPs@Cad-2 combined with laser treatment allowed the lowest number of activated HUVECs across the Matrigel pre-coated transwell (a mimic of extracellular matrix), illustrating the synergistic role of nanoparticle uptake and photothermal treatment in the inhibition of EMC migration. To further demonstrate the importance of nanoparticle-mediated mild hyperthermia, two additional groups were included: Laser only treatment and water-bath heating (a generalized mild hyperthermia at 44°C for 5 min) showed no effect on the cell migration and invasion (**Figure S7**).

Apart from using HUVECs (a dual model for EMCs in atherosclerosis and CAFs in cancer), we also tested the anti-migratory and anti-invasive effects of these treatments using human coronary artery endothelial cells (HCAECs), an exclusive model for studying atherosclerosis.[42] Similar to the results from HUVECs, MelNPs@Cad-2 combined with laser treatment also showed the strongest inhibitory effects on the migration and invasion of activated HCAECs, manifested as the least gap closure % and invaded cell number in 2D and 3D assays, respectively (**Figure 4E-4H**, **Figure S8-S9**). In addition to MelNPs, we also demonstrated similar anti-migration/invasion effects of gold nanorods@Cad-2 and their associated photothermal effect, suggesting the broad applicability of this approach (**Figure S10-S12**). Collectively, these results reveal that MelNPs@Cad-2 with

mild photothermal treatment significantly suppresses the migration and invasion of both activated HUVECs and HCAECs, which offers a potential therapeutic strategy to slow the progression of cancer and atherosclerosis.

Morphological and mechanical characterization of single cells

Since EMCs showed significantly inhibited migration and invasion following the MelNPs@Cad-2 plus laser treatment, we further examined the morphological and mechanical changes of single cells considering these phenotypic properties are closely related to cell motility.

Atomic force microscopy (AFM) was employed to image single, live cells in a liquid, near-physiological environment, where the surface topography and elastic modulus images of individual cells can be collected simultaneously.[28, 43-46] Particularly, the actin cytoskeleton in the dorsal layer of cells was visualized by correlating groove-like features in both topography and modulus channels. As shown in **Figure 5A** and **Figure S13-S15**, the untreated (normal) HUVECs exhibited an elliptical shape with actin cytoskeleton encircling the cell body, a typical trait of low-migratory endothelial cells.[40] In contrast, the activated HUVECs (i.e., EMCs) polarized morphologically into a teardrop shape (with a “big head” and a “small tail”), suggesting they are in the process of active migration. On the cell body, the activated HUVECs displayed stress fibers aligned parallelly to the direction of cell migration, serving to generate contraction force during the cell movement.[47] Importantly, after treating the activated HUVECs with MelNPs@Cad-2 plus laser, the cell morphology returned to the original shape and the stress fibers on the cell body almost disappeared, suggesting the cells reverted to the previous low-migratory state. These observations were also validated by the statistical analysis of AFM images (**Figure 5B-5C**): The aspect ratio of HUVECs underwent an increase from 1.2 to 2.8 following activation and returned to 1.2 after MelNPs@Cad-2 plus laser treatment. Similarly, the average modulus of cells also increased from 10 to 20 kPa and returned to the original level owing to the gain and loss of rigid stress fibers on the cell body.

The cell morphological and cytoskeletal changes were also characterized by super resolution microscopy, by which the ventral actin filaments can be clearly resolved and quantified.[48-50] As shown in **Figure 5D-5E** and **Figure S16-S18**, apart from the cell shape change, the number of stress fibers showed a 2-fold increase after activation and returned to the previous level following the MelNPs@Cad-2 plus laser treatment. In contrast, MelNPs@Cad-2 alone and MelNPs@BSA plus laser can only moderately decrease the stress fibers and cell aspect ratio of activated HUVECs, consistent with their partial migration inhibition (**Figure S19).** Together, the morphological and mechanical characterization of single cells highlight the cytoskeletal change of activated HUVECs after MelNPs@Cad-2 plus laser treatment, in line with the inhibited migration/invasion of EMCs.

Molecular mechanism of inhibited migration/invasion of EMCs

Finally, we delved into the molecular mechanism by which MelNPs@Cad-2 and photothermal treatment inhibit the motility of EMCs. Given our observations on actin cytoskeleton and the important role of cadherin-2 in cell motility, we focused on the cadherin-2 regulated signaling pathway that is associated with the cytoskeleton and cell migration/invasion. Previous studies have shown the positive correlation between surface cadherin-2 and cell migration potential, where cadherin-2 can activate RhoA, a small GTPase that stimulates the assembly of stress fibers and cell migration.[51-52] As schematically shown in **Figure 6A (top)**, RhoA-GDP (the nonactivated form of RhoA) initially binds to P120 which acts as a RhoA inhibitor and prevents RhoA activation.[53-54] However, the tyrosine phosphorylation of P120 (PP120) induced by the membrane cadherin-2 changes the conformation of P120 and enhances the binding affinity of P120 to membrane cadherin-2. The formation of membrane cadherin-2 and PP120 complex weakens the binding of RhoA-GDP with PP120 and releases the RhoA-GDP for its subsequent activation to RhoA-GTP near the membrane. [55-56] Thus, both membrane cadherin-2 and PP120 (tyrosine phosphorylation of P120) are necessary for the activation of RhoA and cell migration.

Given these considerations and our earlier experiments on cell motility, we hypothesize that EMC internalization of MelNPs@Cad-2 should downregulate the membrane cadherin-2 (**Figure 6A, middle**) and photothermal treatment could disrupt the tyrosine phosphorylation of P120 (reducing PP120, **Figure 6A, bottom**), and these two factors contribute synergistically to the reduction of RhoA-GTP, causing loss of stress fibers and inhibited cell migration/invasion. To verify this hypothesis, Western blots were used to quantify the cadherin-2 in different experimental groups including activated HUVECs without treatment (G1), activated HUVECs treated by MelNPs@Cad-2 (G2), and activated HUVECs treated by MelNPs@Cad-2 plus laser (G3). Our experiments showed the membrane cadherin-2 level decreased 30-40% (compared to G1) for both nanoparticle-treated groups (G2 and G3, **Figure 6B**). This is reasonable considering that cellular uptake of cadherin-2 targeted MelNPs@Cad-2 routes the membrane cadherin-2 for lysosomal degradation, in line with the earlier intracellular colocalization images. As expected, the downregulation of membrane cadherin-2 further leads to the reduction of PP120 and RhoA-GTP (**Figure 6C-6F**), accounting for the partially inhibited cell migration/invasion in G2. For the activated HUVECs treated by MelNPs@Cad-2 plus laser (G3), we observed the lowest PP120 and RhoA-GTP levels, suggesting the additional downregulation effects of the photothermal treatment (**Figure 6C-6F**). We infer this could be due to the disruptive effect of photothermal treatment (heat stress) on the intracellular protein phosphorylation, as described earlier.[57-58] Given the positive role of PP120 in RhoA activation, the reduced tyrosine phosphorylation of P120 would lead to the decreased availability of free RhoA-GDP for subsequent activation, resulting in the lowest RhoA-GTP level in G3. Together, membrane cadherin-2 and PP120 (tyrosine phosphorylation of P120), both necessary for the activation of RhoA, can be downregulated by cell uptake of MelNPs@Cad-2 and photothermal treatment, leading to a loss of stress fibers, and inhibited cell migration/invasion.

Conclusions

We have demonstrated that cadherin-2 targeted melanin nanoparticles (MelNPs@Cad-2), combined with mild photothermal treatment, synergistically inhibit the migration and

invasion of endothelial-derived mesenchymal cells (EMCs). This effect is validated using IL-1β activated HUVECs (serving as a dual model for cancer and atherosclerosis) and HCAECs (an atherosclerosis-specific model). Atomic force and super resolution microscopy indicate that this inhibition is accompanied by marked cytoskeletal remodeling — specifically, the loss of actin stress fibers and a morphological transformation from a teardrop to a rounded cell shape — upon treated with MelNPs@Cad-2 and laser irradiation. Further Western blot analyses elucidate the underlying molecular mechanism: internalization of MelNPs@Cad-2 leads to downregulation of membrane cadherin-2, while photothermal treatment disrupts tyrosine phosphorylation of P120 catenin, thereby reducing phosphorylated P120 (PP120) levels. These two events synergistically suppress RhoA-GTP activity, resulting in stress fiber disassembly and impaired cell motility. Given the pivotal role of EMC migration in atherosclerotic plaque formation and the contribution of migratory cancer-associated fibroblasts (approximately 40% derived from EMCs) to tumor metastasis, these in vitro findings serve as a proof-of-concept study for a potential alternative approach to impede both atherosclerosis and cancer progression by targeting EMC migration and invasion. Moreover, considering the broad involvement of cadherin-2 positive EMCs in various cancers, cardiovascular disorders, and fibrotic diseases, this approach may have wide therapeutic applicability in mitigating the progression of EMC-related pathologies.

Methods

Preparation, surface functionalization, and characterization of MelNPs

MelNPs were isolated from cuttlefish ink (Marky's Cuttlefish Squid Ink, Spain) using a gradient centrifugation method. First, 5 g of ink was mixed with 50 mL DI water containing TBS-T (28360, Thermo Fisher) and continuously stirred overnight. The suspension was subjected to an initial centrifugation at 2,000 rpm for 5 minutes and 7,000 rpm for 5 minutes to remove large aggregates and microparticles. Next, the retained supernatant was centrifuged at 12,000 rpm for 10 minutes to collect the desired MelNPs. These MelNPs were washed three times in DI water (10 minutes each wash) to remove food additives in cuttlefish ink and TBS-T.

To prepare MelNPs@PA/BSA, the washed MelNPs were suspended in a 2 mg/mL solution of Protein A and BSA (77673, Thermo Fisher, and A7030, Sigma-Aldrich, mixed in a 1:3 mass ratio) in Na_2HPO_4/NaH_2PO_4 buffer (pH 8-9) and incubated for overnight under continuous shaking. Then the nanoparticles were washed (3x) with DI water (12,000 rpm, 10 minutes each wash). For the preparation of MelNPs@PA/BSA@Cad-2, MelNPs@PA/BSA were incubated with cadherin-2 antibody (13116S, Cell Signaling Technology, 100 μg/mL in PBS) for 1 hour, followed by 3x washes with PBS (12,000 rpm, 10 minutes per wash). To prepare MelNPs@BSA, the isolated MelNPs were suspended in a 2 mg/mL solution of BSA in Na_2HPO_4/NaH_2PO_4 buffer (pH 8-9) and incubated for overnight under continuous shaking. Then the particles were washed 3x with DI water (12,000 rpm, 10 minutes each wash).

The morphology of unmodified MelNPs and antibody modified MelNPs@Cad-2 was investigated using a JEOL JEM-2100. The hydrodynamic size and zeta potential of MelNPs were determined by a Malvern Zetasizer Nano ZS. The absorbance spectra of MelNPs in various solutions were measured using a Shimadzu-1900 UV-Vis spectrophotometer. The temperature elevation of the nanoparticle suspension under 808 nm laser irradiation (0.5 W/cm^2) was measured using an infrared thermometer (Thermo Fisher).

Cell culture

Human umbilical vein endothelial cells (PCS-100-010, HUVECs), human coronary artery endothelial cells (PCS-100-020, HCAECs), vascular cell basal medium, endothelial cell growth kit-VEGF, trypsin-EDTA, and trypsin neutralizing solution were obtained from ATCC. Both cells were cultured in the same medium and growth kit.

Cytotoxicity assays

HUVECs were seeded in 96-well plates (5,000 cells/well) and incubated for 24 hours. Then the medium was removed and replaced with 100 μL medium containing 100 μg/mL MelNPs@BSA or MelNPs@Cad-2 for another 12 hours of culturing. For the laser treated groups, the cells with nanoparticles in medium were further irradiated with the laser for 5 min (0.5 W/cm^2). Subsequently, cytotoxicity assays were carried out using the MTT Cell Viability Assay Kit (V13154, Thermo Fisher) and the LDH Cytotoxicity Assay Kit (C20301, Thermo Fisher). Absorbance measurements were conducted using a BioTek Epoch 2 plate reader.

Immunostaining of cadherin-2

Untreated HUVECs were seeded in 50 mm glass-bottom dishes and incubated in normal medium for 24 hours. For IL-1β activated HUVECs, after 12 hours in normal medium, IL-1β (10 ng/mL, 201-LB, R&D System) contained medium was used to culture cells for another 12 hours. The cells were then fixed with paraformaldehyde (28908, Thermo Fisher) for 5 minutes, and blocked by BlockAid solution (B10710, Thermo Fisher) for 30 minutes. Next, the cells were incubated overnight with cadherin-2 antibody (13116S, CST, Rabbit IgG) diluted 1:1000 in BlockAid solution. After incubation, the cells were washed 3x with DPBS and incubated for 30 minutes with Alexa Fluor 488-conjugated anti-rabbit IgG (4412S, CST) diluted 1:2000 in BlockAid solution, followed by another three washes

with DPBS. Fluorescence imaging was conducted by an Olympus IX71 microscope. Quantitative analysis of cahherin-2 level on the cell surface was conducted by analyzing total fluorescence intensity of individual cell using the ImageJ software.

Cellular uptake and intracellular localization of MelNPs

HUVECs were seeded in 50 mm glass-bottom dishes and incubated for 12 hours. For the normal HUVEC groups, cell medium was switched to fresh normal medium and incubated for another 12 hours. For the activated HUVEC groups, cell medium was switched to medium containing 10 ng/mL IL-1β and incubated for another 12 hours. Subsequently, the medium was replaced with medium containing 100 μg/mL MelNPs@BSA or MelNPs@Cad-2 and the cells were incubated with nanoparticles for 12 hours. After fixation, the cellular uptake of MelNPs was quantified by measuring the total grayscale grade intensity using the ImageJ software. Five random areas were analyzed for each experimental group. To assess the intracellular localization of MelNPs@Cad-2, following nanoparticle uptake, the cells were stained with LysoTracker (L7528, Thermo Fisher). Bright field imaging and fluorescence imaging were conducted by an Olympus IX71 microscope.

2D migration and 3D invasion assays

HUVECs and HCAECs were seed in 12-well plates and incubated for 12 hours. For nonactivated (normal) groups, cell medium was switched to fresh normal medium and incubated for another 12 hours. For activated HUVECs and HCAECs, cell medium was switched to medium with 10 ng/mL IL-1β and cells were cultured for another 12 hours. Subsequently, the medium was replaced with medium containing 100 μg/mL MelNPs@BSA or MelNPs@Cad-2, and cells were incubated with nanoparticles for 12 hours. For the laser-treated groups, following nanoparticle incubation, cells were exposed to the laser at an intensity of 0.5 W/cm² for 5 minutes. After treatments, a pipet tip was used to scrape a gap in each well, followed by five washes to remove floating cells. Images around the gap area were captured immediately after the scraping was made (time 0 h) and 9 hours later. The cell migration capability was assessed by the % of gap closure over 9 hours. For the 3D invasion assay, 2% Matrigel (Corning) was first diluted with serum-free cell medium and 50 μL of this solution was added to each insert. HUVECs and HCAECs were then seeded in the inserts. Serum-free medium and serum-rich medium were used over and under the inserts, respectively. After waiting for 17 hours, the inserts were stained with Crystal Violet (in methanol) and the invaded cells across the inserts were quantified.

AFM and super resolution imaging

The detailed imaging parameters can be found in our previous publications.[28, 59-60] In brief, for AFM imaging, untreated or treated cells were seeded into 60 mm dishes and imaged at 37 °C in normal medium using a Bruker BioScope Resolve AFM under a nanomechanical mode with PFQNM-LC-A-CAL probes. The imaging was operated within a vertical oscillation range of 300-600 nm, an indentation force of 800-1000 pN, a scan frequency of 0.12 Hz and a resolution of 256 × 256 pixels. The acquired AFM images were processed and analyzed using NanoScope Analysis software to generate modulus images. To prepare super resolution imaging, untreated or treated cells were fixed with

paraformaldehyde, permeabilized with Triton X-100 in cytoskeletal buffer, blocked with 1% BSA for 30 minutes at 37°C, and stained with 0.5 μM Alexa Fluor 568 phalloidin (Thermo Fisher). The super resolution imaging was conducted in imaging buffer with a fluorescence microscope (Olympus IX81) and a 100x TIRF objective. The imaging data were processed and analyzed using Thunder-STORM in ImageJ.

Western blots

For Western blot analysis, cell lysis proteins were separated on SDS-PAGE gels at 150 V for 30 minutes in 1x running buffer (1610772, BioRad). The membrane proteins were extracted using Mem-PER Plus Membrane Protein Extraction Kit (89842, Thermo Fisher). After SDS separation, the proteins were transferred onto nitrocellulose membranes using the Biorad Trans-Blot Turbo Transfer System. To block nonspecific binding, the membranes were treated with EveryBlot blocking buffer (12010020, BioRad). Primary antibodies, diluted as recommended, were used to immerse the membranes for 12 hours. Then secondary antibodies were used to treat the membrane for 1 hour. Protein bands were imaged using the ChemiDoc Imaging System (BioRad). RIPA buffer (89900, Thermo Fisher) was used to process cells for quantifying cadherin-2, total p120, and total RhoA. Activated RhoA-GTP was quantified after isolation using the Active Rho Kit (16116, Thermo Fisher Scientific). Tyrosine-phosphorylated p120 (pp120) was isolated by combining p120 antibody, a tyrosine phosphorylation antibody, with an immunoprecipitation kit (26149, Thermo Fisher Scientific).

Schematic illustration/artwork

Schematic illustration/artwork was created by authors using BioRender.

Supporting Information

Examples of immunofluorescence staining images, cellular uptake images, migration and invasion assays, photothermal effect of gold nanorods, calculation of gold nanorods concentration, AFM and super resolution images, and raw data of Western blots.

Acknowledgments

This work is supported by the National Science Foundation CAREER Award (2143972) and the National Institutes of Health AREA Award (R15CA274349).

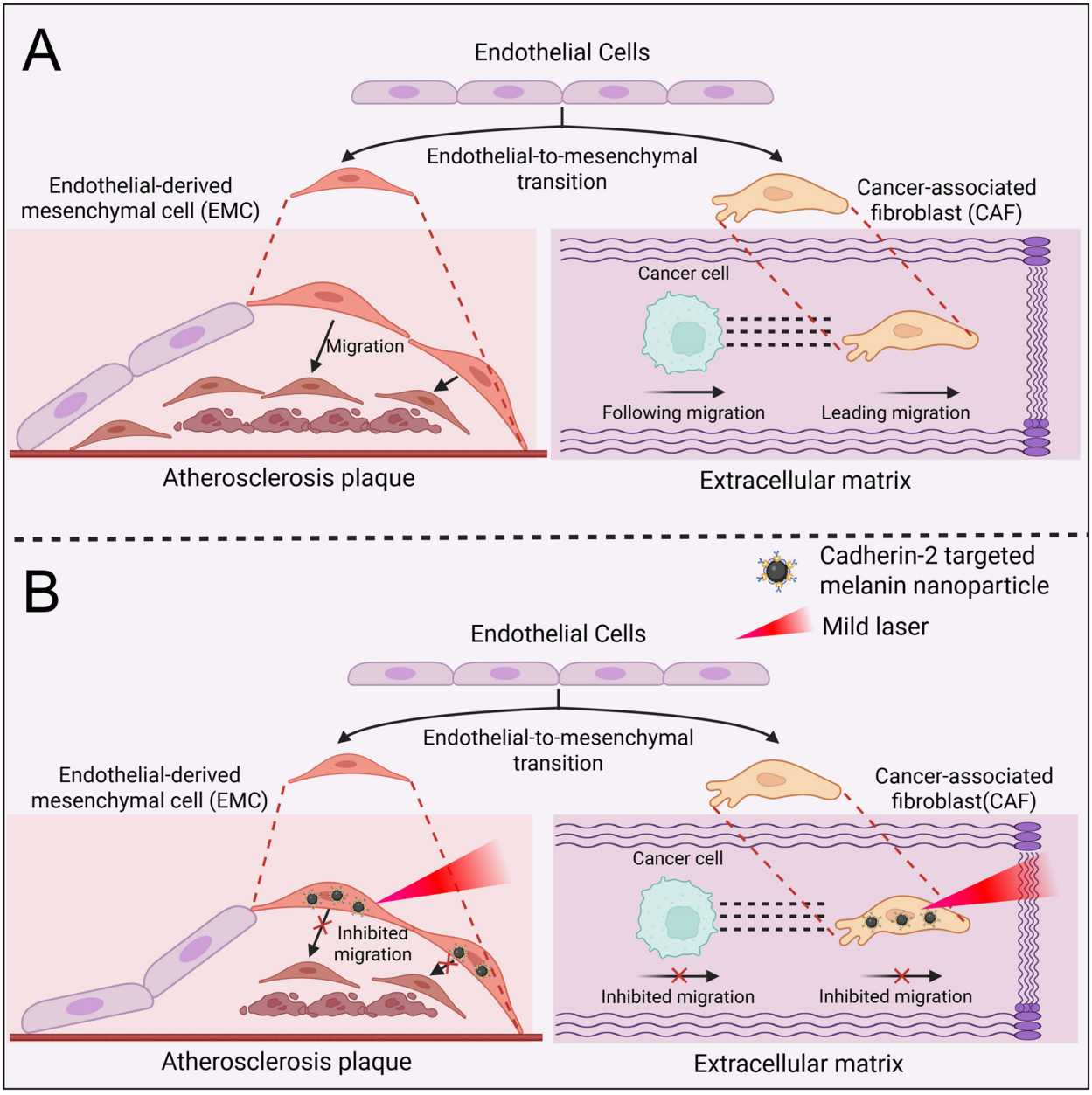

Figure 1. The overall concept of this work. (A) Schematic illustrating that the migration of EMCs and CAFs (derived from endothelial-to-mesenchymal transition) contributes significantly to atherosclerosis plaque buildup and cancer cell migration, respectively. (B) Schematic illustrating that cadherin-2 targeted melanin nanoparticles and their photothermal effect (*via* laser irradiation) can target EMCs/CAFs and inhibit their migration to hamper the atherosclerosis plaque formation and cancer metastasis.

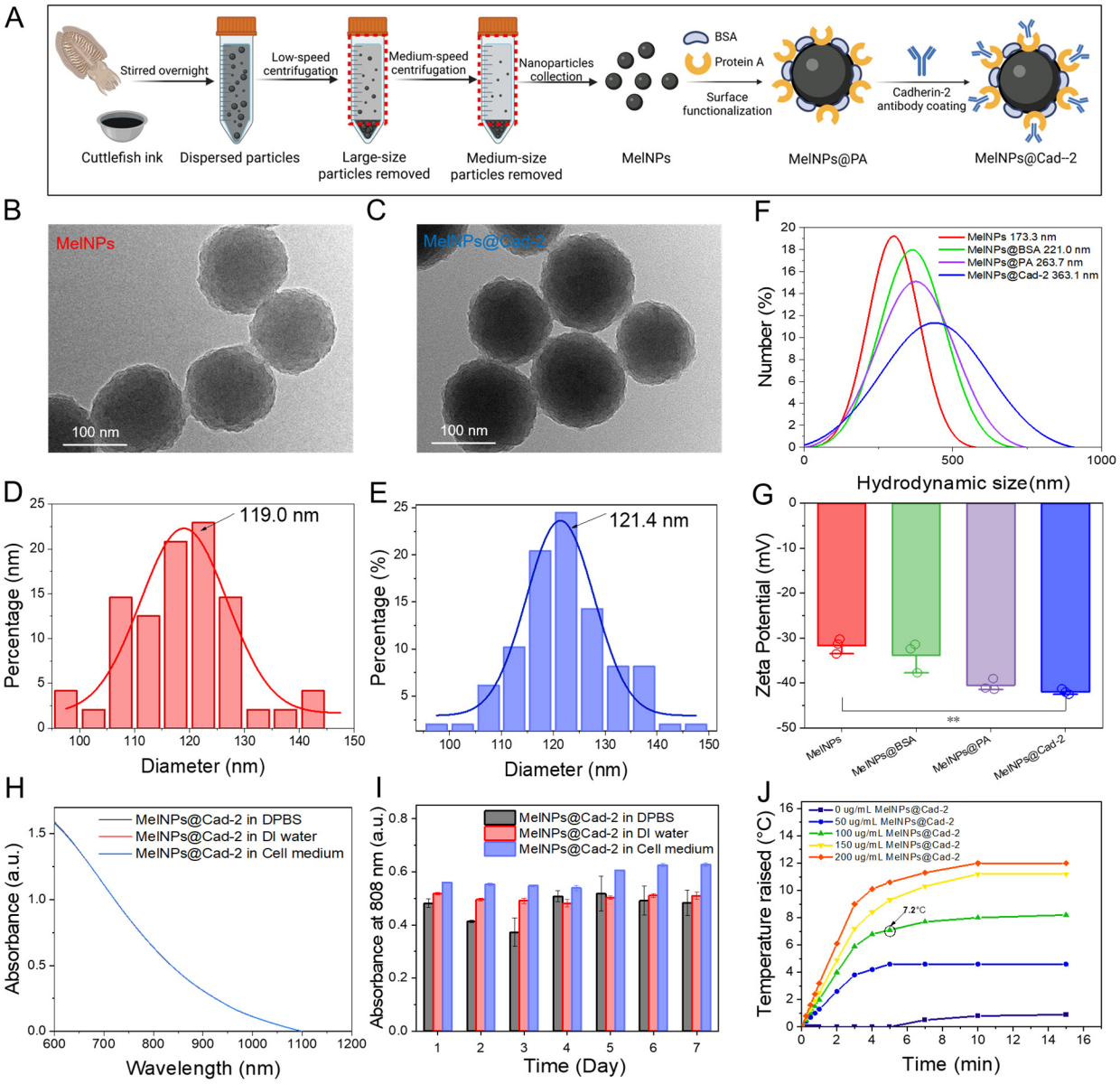

Figure 2. Preparation and characterization of cadherin-2 targeted melanin nanoparticles. (A) The workflow of extraction and surface functionalization of MelNPs. (B-C) Transmission electron microscopy (TEM) images of MelNPs and cadherin-2 antibody-functionalized MelNPs (MelNPs@Cad-2). (D-E) Statistical analysis of the nanoparticle size distribution from TEM images. (F-G) Hydrodynamic size and Zeta potential of bare MelNPs, MelNPs@PA, MelNPs@BSA, and MelNPs@Cad-2 in water. Data are plotted as mean ± SD, n=3. **< 0.01. (H) Absorption spectra of MelNPs@Cad-2 (100 μg/mL) in water, DPBS, and cell medium. (I) 808 nm absorbance of MelNPs@Cad-2 (100 μg/mL) in the three media monitored during a 7-day period. Data are plotted as mean ± SD, n=5. (J) The temperature increases of cell media containing MelNPs@Cad-2 upon 808 nm laser irradiation.

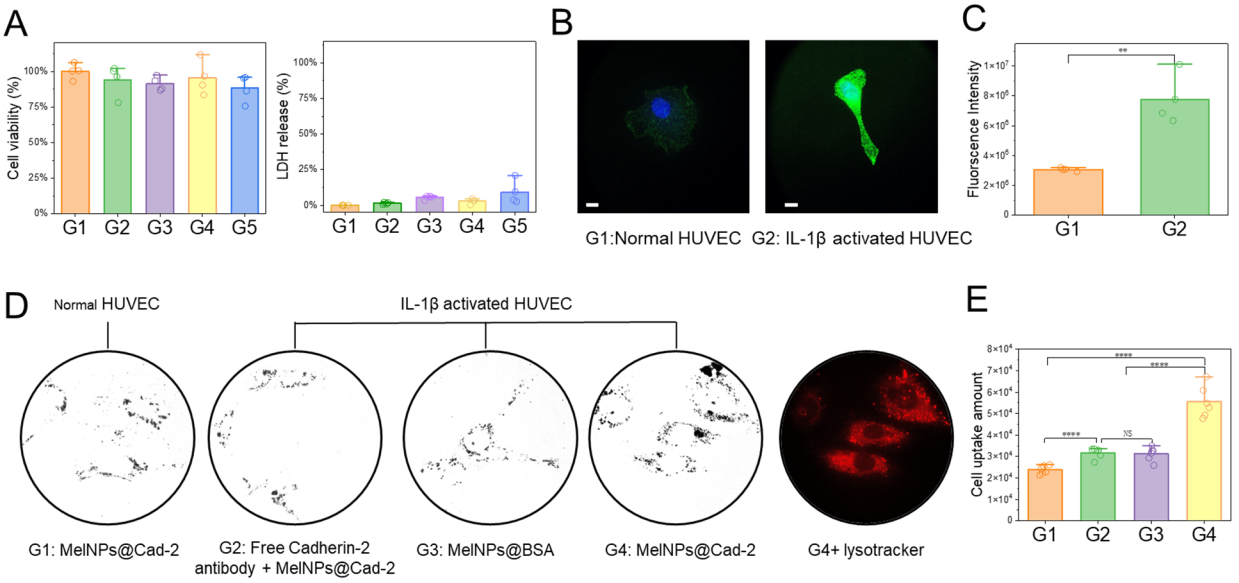

Figure 3. Biocompatibility and EMC-targeting ability of MelNPs@Cad-2. (A) MTT and LDH assays assessing cell viability and membrane damage of HUVECs after different treatments: G1: normal cell medium; G2: MelNPs@BSA; G3: MelNPs@BSA + Laser; G4: MelNPs@Cad-2; and G5: MelNPs@Cad-2 + Laser. Data are plotted as mean ± SD, n=4. (B) Immunofluorescence staining of surface cadherin-2 on normal (G1) and IL-1β-activated (G2) HUVECs. Scale bar: 10 μm. (C) Statistical analysis of fluorescence intensity of surface cadherin-2 on both HUVECs. Data are plotted as mean ± SD, n=4, **<0.01. (D) Bright field images of cell uptake of MelNPs under different conditions. Lysotracker red fluorescence corresponds to G4: activated HUVECs after incubation with MelNPs@Cad-2. (E) The cell uptake of nanoparticles in bright field images quantified by measuring the grayscale values in the field of view. Data are plotted as mean ± SD, n=6, NS>0.05, ****<0.0001.

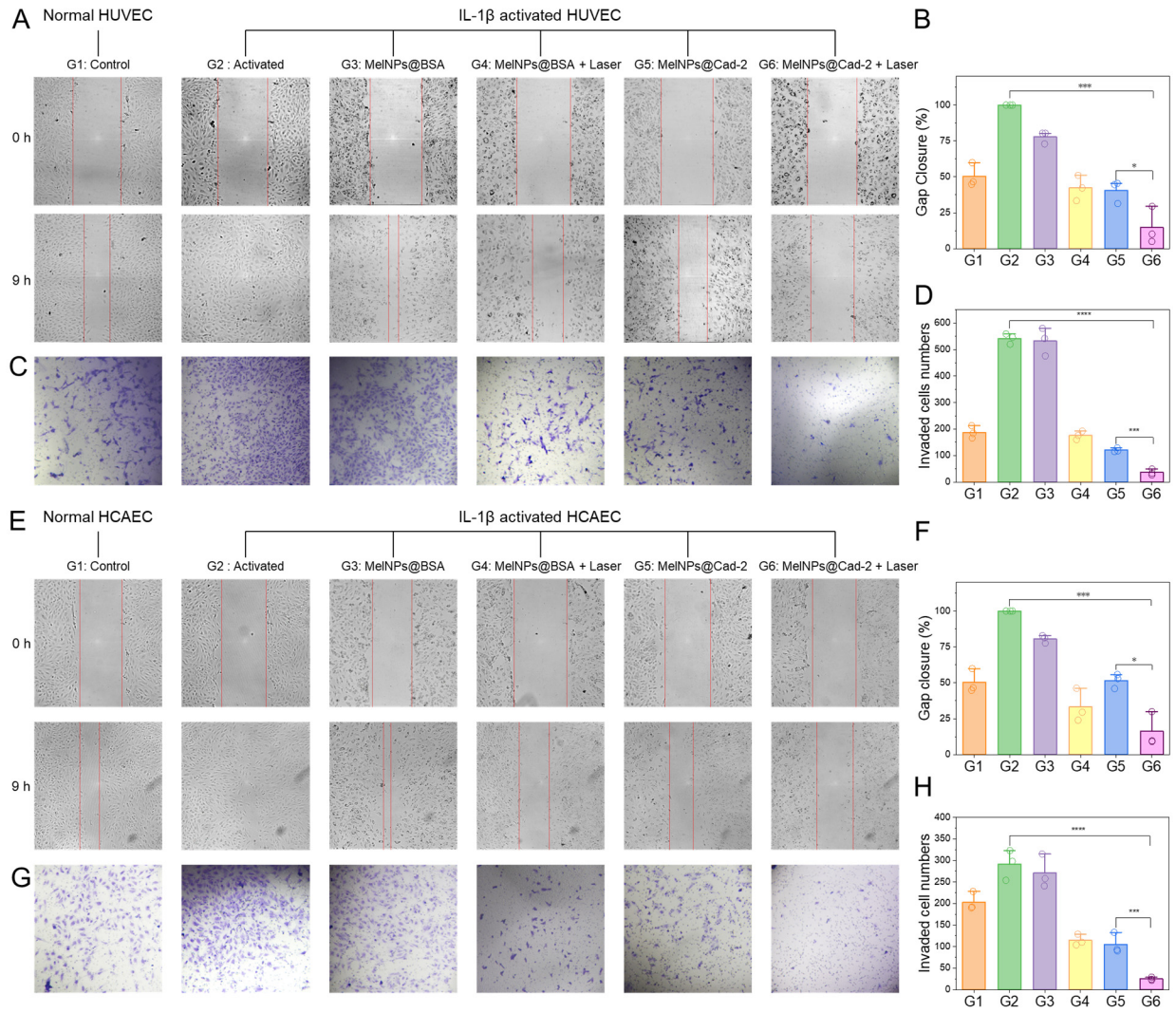

Figure 4. Anti-migration/invasion effects of MelNPs@Cad-2 and photothermal treatment. (A-B) 2D migration assays assessing HUVEC migration in different groups. (C-D) 3D invasion assays assessing HUVEC invasion in different groups. (E-F) 2D migration assays assessing HCAEC migration under different treatments. (G-H) 3D invasion assays assessing HCAEC invasion under different treatments. Data are plotted as mean ± SD, n=3, ****<0.0001, ***< 0.001, *< 0.05.

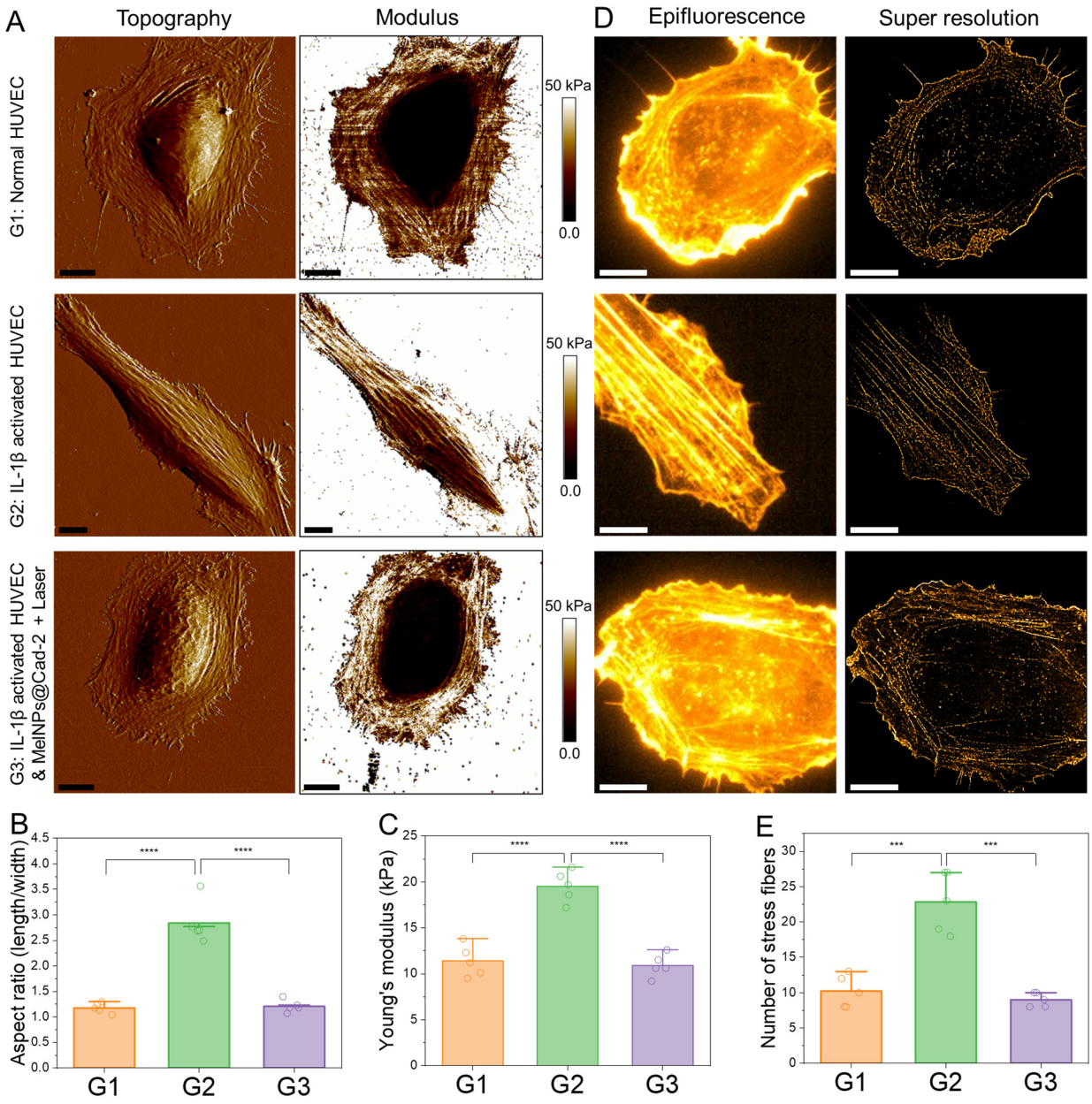

Figure 5. Morphological and mechanical characterization of single cells. (A) AFM nanomechanical imaging of single HUVECs in different treatment groups. Left panel: Topography map. Right panel: Young's modulus map. Scale bar: 10 μm. (B-C) The aspect ratio and average Young's modulus of single cells analyzed using AFM images. (D) Super resolution imaging of actin cytoskeleton in HUVECs. Left panel: Conventional epifluorescence image. Right panel: Super resolution image. Scale bar: 10 μm. (E) The number of stress fibers in single cells analyzed using super resolution images. Data are plotted as mean ± SD, n=5, ****<0.0001, ***< 0.001.

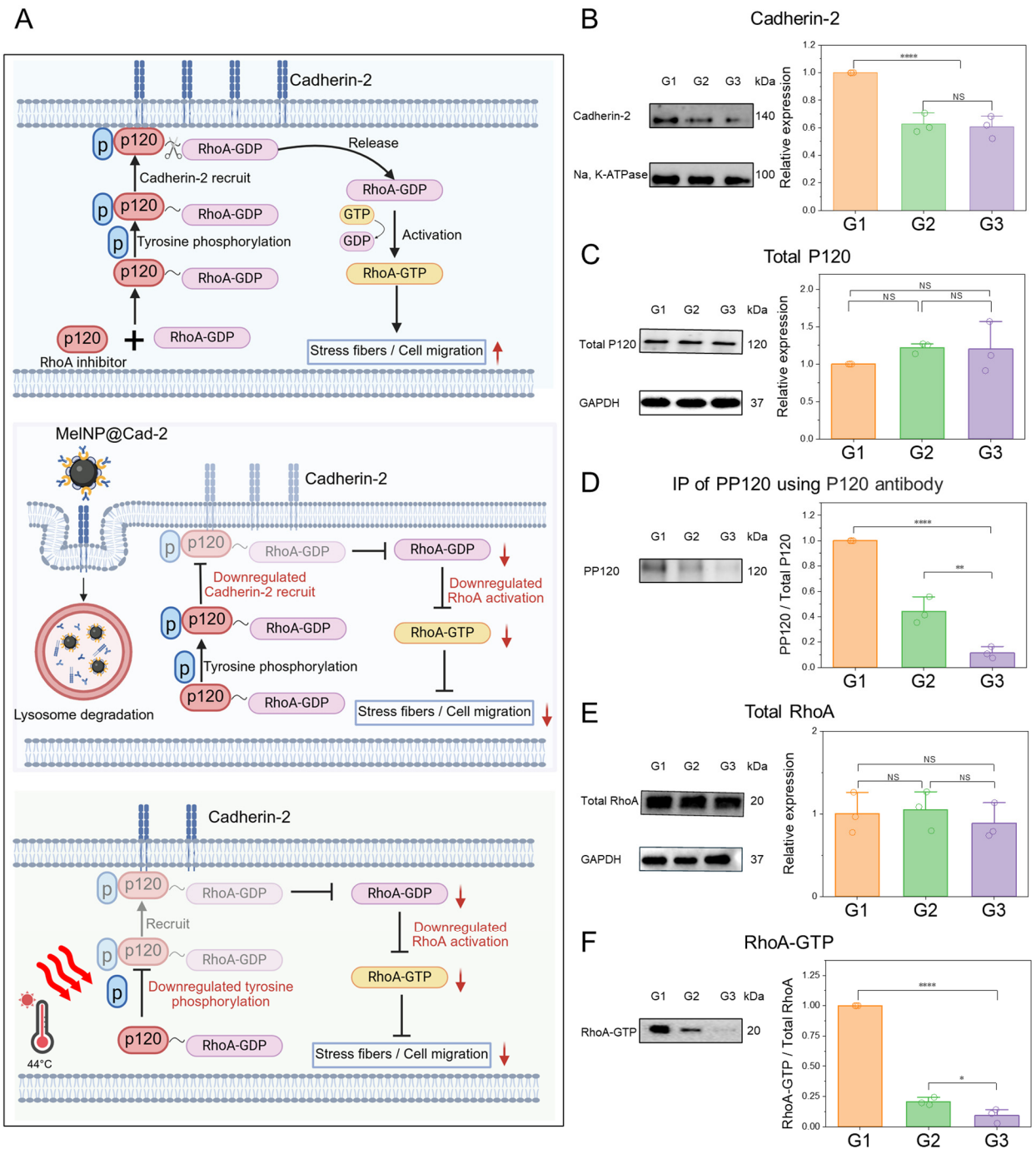

Figure 6. Molecular mechanism of inhibited migration/invasion of EMCs. (A) Schematic illustration of how MeINPs@Cad-2 and photothermal treatment inhibited the migration and invasion of EMCs. (B-F) Western blot analysis of membrane cadherin-2, total P120, tyrosine-phosphorylated p120 (PP120), total RhoA, and RhoA-GTP in HUVECs under different treatment groups: G1: IL-1β activated HUVECs; G2: IL-1β activated HUVECs treated with MeINPs@Cad-2; G3: IL-1β activated HUVECs treated with MeINPs@Cad-2 and laser. Na/K-ATPase and GAPDH serves as loading controls. Data are plotted as mean ± SD, n=3, NS>0.05, ****<0.0001, *< 0.05.

References

1. Bischoff, J., Endothelial-to-Mesenchymal Transition. *Circulation Research* **2019,** *124* (8), 1163-1165.
2. Kovacic, J. C.; Dimmeler, S.; Harvey, R. P.; Finkel, T.; Aikawa, E.; Krenning, G.; Baker, A. H., Endothelial to Mesenchymal Transition in Cardiovascular Disease: JACC State-o -the-Art Review. *Journal of the American College of Cardiology* **2019,** *73* (2), 190-209.
3. Clere, N.; Renault, S.; Corre, I., Endothelial-to-Mesenchymal Transition in Cancer. *Frontiers in Cell and Developmental Biology* **2020,** *8*.
4. Choi, K. J.; Nam, J.-K.; Kim, J.-H.; Choi, S.-H.; Lee, Y.-J., Endothelial-to-mesenchymal transition in anticancer therapy and normal tissue damage. *Experimental & Molecular Medicine* **2020,** *52* (5), 781-792.
5. Piera-Velazquez, S.; Jimenez, S. A., Endothelial to Mesenchymal Transition: Role in Physiology and in the Pathogenesis o Human Diseases. *Physiological reviews* **2019,** *99* (2), 1281-1324.
6. Souilhol, C.; Harmsen, M. C.; Evans, P. C.; Krenning, G., Endothelial-mesenchymal transition in atherosclerosis. *Cardiovascular research* **2018,** *114* (4), 565-577.
7. Liu, S.; Xu, D. S.; Li, M.; Zhang, Y.; Li, Q.; Li, T. T.; Ren, L. Q., Icariin attenuates endothelial-mesenchymal transition via H19/miR-148b-3p/ELF5 in ox-LDL-stimulated HUVECs. *Molecular therapy. Nucleic acids* **2021,** *23*, 464-475.
8. Potenta, S.; Zeisberg, E.; Kalluri, R., The role o endothelial-to-mesenchymal transition in cancer progression. *British journal of cancer* **2008,** *99* (9), 1375-9.
9. Baschieri, F.; Illand, A.; Barbazan, J.; Zajac, O.; Henon, C.; Loew, D.; Dingli, F.; Vignjevic, D. M.; Lévêque-Fort, S.; Montagnac, G., Fibroblasts generate topographical cues that steer cancer cell migration. *Science advances* **2023,** *9* (33), eade2120.
10. Liu, T.; Zhou, L.; Li, D.; Andl, T.; Zhang, Y., Cancer-Associated Fibroblasts Build and Secure the Tumor Microenvironment. *Frontiers in Cell and Developmental Biology* **2019,** *7*.
11. Goliwas, K. F.; Libring, S.; Berestesky, E.; Gholizadeh, S.; Schwager, S. C.; Frost, A. R.; Gaborski, T. R.; Zhang, J.; Reinhart-King, C. A., Mitochondrial trans er rom cancer-associated fibroblasts increases migration in aggressive breast cancer. *Journal of cell science* **2023,** *136* (14).
12. Xu, F.; Guo, H.; Zustiak, S. P.; Genin, G. M., Targeting the physical microenvironment o tumors or drug and immunotherapy. *Advanced drug delivery reviews* **2023,** *196*, 114768.
13. Cords, L.; Engler, S.; Haberecker, M.; Rüschoff, J. H.; Moch, H.; de Souza, N.; Bodenmiller, B., Cancer-associated fibroblast phenotypes are associated with patient outcome in non-small cell lung cancer. *Cancer cell* **2024,** *42* (3), 396-412.e5.
14. Evrard, S. M.; Lecce, L.; Michelis, K. C.; Nomura-Kitabayashi, A.; Pandey, G.; Purushothaman, K. R.; d'Escamard, V.; Li, J. R.; Hadri, L.; Fujitani, K.; Moreno, P. R.; Benard, L.; Rimmele, P.; Cohain, A.; Mecham, B.; Randolph, G. J.; Nabel, E. G.; Hajjar, R.; Fuster, V.; Boehm, M.; Kovacic, J. C., Endothelial to mesenchymal transition is common in atherosclerotic lesions and is associated with plaque instability. *Nature communications* **2016,** *7*, 11853.
15. Ma, J.; Sanchez-Duffhues, G.; Goumans, M.-J.; ten Dijke, P., TGF-β-Induced Endothelial to Mesenchymal Transition in Disease and Tissue Engineering. *Frontiers in Cell and Developmental Biology* **2020,** *8*.
16. Man, S.; Sanchez Duffhues, G.; ten Dijke, P.; Baker, D., The therapeutic potential o targeting the endothelial-to-mesenchymal transition. *Angiogenesis* **2019,** *22* (1), 3-13.
17. Luo, L.; Zhang, B.; Tao, F.; Chen, Z.; Ye, Q.; Zhao, X.; Wu, J., Perfluorotributylamine-Loaded Albumin Nanoparticles Downregulate Platelet-Derived TGFβ to Inhibit Tumor Metastasis. *ACS Nano* **2023,** *17* (16), 15388-15400.

18. Ridker Paul, M.; Everett Brendan, M.; Thuren, T.; MacFadyen Jean, G.; Chang William, H.; Ballantyne, C.; Fonseca, F.; Nicolau, J.; Koenig, W.; Anker Ste an, D.; Kastelein John, J. P.; Cornel Jan, H.; Pais, P.; Pella, D.; Genest, J.; Ci kova, R.; Lorenzatti, A.; Forster, T.; Kobalava, Z.; Vida-Simiti, L.; Flather, M.; Shimokawa, H.; Ogawa, H.; Dellborg, M.; Rossi Paulo, R. F.; Troquay Roland, P. T.; Libby, P.; Glynn Robert, J., Antiinflammatory Therapy with Canakinumab or Atherosclerotic Disease. *New England Journal of Medicine 377* (12), 1119-1131.
19. Flores, A. M.; Hosseini-Nassab, N.; Jarr, K.-U.; Ye, J.; Zhu, X.; Wirka, R.; Koh, A. L.; Tsantilas, P.; Wang, Y.; Nanda, V.; Kojima, Y.; Zeng, Y.; Lotfi, M.; Sinclair, R.; Weissman, I. L.; Ingelsson, E.; Smith, B. R.; Leeper, N. J., Pro-efferocytic nanoparticles are specifically taken up by lesional macrophages and prevent atherosclerosis. *Nature Nanotechnology* **2020,** *15* (2), 154-161.
20. Krizbai, I. A.; Gasparics, Á.; Nagyőszi, P.; Fazakas, C.; Molnár, J.; Wilhelm, I.; Bencs, R.; Rosivall, L.; Sebe, A., Endothelial-mesenchymal transition o brain endothelial cells: possible role during metastatic extravasation. *PloS one* **2015,** *10* (3), e0119655.
21. Gaikwad, A. V.; Lu, W.; Dey, S.; Bhattarai, P.; Haug, G.; Larby, J.; Chia, C.; Jaffar, J.; Westall, G.; Singhera, G. K.; Hackett, T.-L.; Eapen, M. S.; Sohal, S. S., Endothelial-to-mesenchymal transition: a precursor to pulmonary arterial remodelling in patients with idiopathic pulmonary fibrosis. *ERJ Open Research* **2023,** *9* (2), 00487-2022.
22. Seth, A.; Gholami Derami, H.; Gupta, P.; Wang, Z.; Rathi, P.; Gupta, R.; Cao, T.; Morrissey, J. J.; Singamaneni, S., Polydopamine–Mesoporous Silica Core–Shell Nanoparticles or Combined Photothermal Immunotherapy. *ACS Applied Materials & Interfaces* **2020,** *12* (38), 42499-42510.
23. Shen, S.; Gao, Y.; Ouyang, Z.; Jia, B.; Shen, M.; Shi, X., Photothermal-triggered dendrimer nanovaccines boost systemic antitumor immunity. *Journal of Controlled Release* **2023,** *355*, 171-183.
24. Hu, W.; Xiao, T.; Li, D.; Fan, Y.; Xing, L.; Wang, X.; Li, Y.; Shi, X.; Shen, M., Intelligent Molybdenum Disulfide Complexes as a Plat orm or Cooperative Imaging-Guided Tri-Mode Chemo-Photothermo-Immunotherapy. *Advanced Science* **2021,** *8* (14), 2100165.
25. Li, J.; Hu, Y.; Yang, J.; Wei, P.; Sun, W.; Shen, M.; Zhang, G.; Shi, X., Hyaluronic acid-modified Fe3O4@Au core/shell nanostars or multimodal imaging and photothermal therapy o tumors. *Biomaterials* **2015,** *38*, 10-21.
26. Wang, H.; Chang, J.; Shi, M.; Pan, W.; Li, N.; Tang, B., A Dual-Targeted Organic Photothermal Agent or Enhanced Photothermal Therapy. *Angewandte Chemie International Edition* **2019,** *58* (4), 1057-1061.
27. Shi, M.; Fu, Z.; Pan, W.; Chen, Y.; Wang, K.; Zhou, P.; Li, N.; Tang, B., A Protein-Binding Molecular Photothermal Agent or Tumor Ablation. *Angewandte Chemie International Edition* **2021,** *60* (24), 13564-13568.
28. Liu, J.; Smith, S.; Wang, C., Reversing the Epithelial–Mesenchymal Transition in Metastatic Cancer Cells Using CD146-Targeted Black Phosphorus Nanosheets and a Mild Photothermal Treatment. *ACS Nano* **2022,** *16* (2), 3208-3220.
29. Evrard, S. M.; Lecce, L.; Michelis, K. C.; Nomura-Kitabayashi, A.; Pandey, G.; Purushothaman, K. R.; d'Escamard, V.; Li, J. R.; Hadri, L.; Fujitani, K.; Moreno, P. R.; Benard, L.; Rimmele, P.; Cohain, A.; Mecham, B.; Randolph, G. J.; Nabel, E. G.; Hajjar, R.; Fuster, V.; Boehm, M.; Kovacic, J. C., Endothelial to mesenchymal transition is common in atherosclerotic lesions and is associated with plaque instability. *Nature communications* **2016,** *7* (1), 11853.
30. Choi, S.-H.; Kim, A. R.; Nam, J.-K.; Kim, J.-M.; Kim, J.-Y.; Seo, H. R.; Lee, H.-J.; Cho, J.; Lee, Y.-J., Tumour-vasculature development via endothelial-to-mesenchymal transition a ter radiotherapy controls CD44v6+ cancer cell and macrophage polarization. *Nature communications* **2018,** *9* (1), 5108.

31. Deng, R.-H.; Zou, M.-Z.; Zheng, D.; Peng, S.-Y.; Liu, W.; Bai, X.-F.; Chen, H.-S.; Sun, Y.; Zhou, P.-H.; Zhang, X.-Z., Nanoparticles rom Cuttlefish Ink Inhibit Tumor Growth by Synergizing Immunotherapy and Photothermal Therapy. *ACS Nano* **2019,** *13* (8), 8618-8629.
32. Gholami Derami, H.; Gupta, P.; Weng, K.-C.; Seth, A.; Gupta, R.; Silva, J. R.; Raman, B.; Singamaneni, S., Reversible Photothermal Modulation o Electrical Activity o Excitable Cells using Polydopamine Nanoparticles. *Advanced Materials* **2021,** *33* (32), 2008809.
33. Qiu, J.; Shi, Y.; Xia, Y., Polydopamine Nanobottles with Photothermal Capability or Controlled Release and Related Applications. *Advanced Materials* **2021,** *33* (45), 2104729.
34. Liu, J.; Yu, X.; Braucht, A.; Smith, S.; Wang, C., N-Cadherin Targeted Melanin Nanoparticles Reverse the Endothelial–Mesenchymal Transition in Vascular Endothelial Cells to Potentially Slow the Progression o Atherosclerosis and Cancer. *ACS Nano* **2024,** *18* (11), 8229-8247.
35. Reymond, N.; d'Água, B. B.; Ridley, A. J., Crossing the endothelial barrier during metastasis. *Nature Reviews Cancer* **2013,** *13* (12), 858-870.
36. Medina-Leyte, D. J.; Domínguez-Pérez, M.; Mercado, I.; Villarreal-Molina, M. T.; Jacobo-Albavera, L., Use o Human Umbilical Vein Endothelial Cells (HUVEC) as a Model to Study Cardiovascular Disease: A Review. *Applied Sciences* **2020,** *10* (3), 938.
37. Huang, Q.; Gan, Y.; Yu, Z.; Wu, H.; Zhong, Z., Endothelial to Mesenchymal Transition: An Insight in Atherosclerosis. *Frontiers in cardiovascular medicine* **2021,** *8*, 734550.
38. Pérez, L.; Muñoz-Durango, N.; Riedel, C. A.; Echeverría, C.; Kalergis, A. M.; Cabello-Verrugio, C.; Simon, F., Endothelial-to-mesenchymal transition: Cytokine-mediated pathways that determine endothelial fibrosis under inflammatory conditions. *Cytokine & Growth Factor Reviews* **2017,** *33*, 41-54.
39. Qian, C.; Dong, G.; Yang, C.; Zheng, W.; Zhong, C.; Shen, Q.; Lu, Y.; Zhao, Y., Broadening horizons: molecular mechanisms and disease implications o endothelial-to-mesenchymal transition. *Cell Communication and Signaling* **2025,** *23* (1), 16.
40. Sánchez-Duffhues, G.; García de Vinuesa, A.; ten Dijke, P., Endothelial-to-mesenchymal transition in cardiovascular diseases: Developmental signaling pathways gone awry. *Developmental Dynamics* **2018,** *247* (3), 492-508.
41. Alvandi, Z.; Bischoff, J., Endothelial-mesenchymal transition in cardiovascular disease. *Arteriosclerosis, Thrombosis, and Vascular Biology* **2021,** *41* (9), 2357-2369.
42. Cardona-Mendoza, A.; Roa Molina, N. S.; Castillo, D. M.; La aurie, G. I.; Gualtero Escobar, D. F., Human Coronary Artery Endothelial Cell Response to Porphyromonas gingivalis W83 in a Collagen Three-Dimensional Culture Model. *Microorganisms* **2024,** *12* (2).
43. Kota, D.; Kang, L.; Rickel, A.; Liu, J.; Smith, S.; Hong, Z.; Wang, C., Low doses o zeolitic imidazolate ramework-8 nanoparticles alter the actin organization and contractility o vascular smooth muscle cells. *Journal of Hazardous Materials* **2021,** *414*, 125514.
44. Calzado-Martín, A.; Encinar, M.; Tamayo, J.; Calleja, M.; San Paulo, A., Effect o Actin Organization on the Stiffness o Living Breast Cancer Cells Revealed by Peak-Force Modulation Atomic Force Microscopy. *ACS Nano* **2016,** *10* (3), 3365-3374.
45. Dumitru, A. C.; Poncin, M. A.; Conrard, L.; Du rêne, Y. F.; Tyteca, D.; Alsteens, D., Nanoscale membrane architecture o healthy and pathological red blood cells. *Nanoscale Horizons* **2018,** *3* (3), 293-304.
46. Eghiaian, F.; Rigato, A.; Scheuring, S., Structural, Mechanical, and Dynamical Variability o the Actin Cortex in Living Cells. *Biophysical Journal* **2015,** *108* (6), 1330-1340.
47. Wang, M.; Cheng, B.; Yang, Y.; Liu, H.; Huang, G.; Han, L.; Li, F.; Xu, F., Microchannel Stiffness and Confinement Jointly Induce the Mesenchymal-Amoeboid Transition o Cancer Cell Migration. *Nano Letters* **2019,** *19* (9), 5949-5958.

48. van de Linde, S.; Löschberger, A.; Klein, T.; Heidbreder, M.; Wolter, S.; Heilemann, M.; Sauer, M., Direct stochastic optical reconstruction microscopy with standard fluorescent probes. *Nature Protocols* **2011,** *6* (7), 991-1009.
49. Dempsey, G. T.; Vaughan, J. C.; Chen, K. H.; Bates, M.; Zhuang, X., Evaluation o fluorophores or optimal per ormance in localization-based super-resolution imaging. *Nature Methods* **2011,** *8* (12), 1027-1036.
50. Xu, J.; Ma, H.; Liu, Y., Stochastic Optical Reconstruction Microscopy (STORM). *Current Protocols in Cytometry* **2017,** *81* (1), 12.46.1-12.46.27.
51. Taulet, N.; Comunale, F.; Favard, C.; Charrasse, S.; Bodin, S.; Gauthier-Rouvière, C., N-cadherin/p120 catenin association at cell-cell contacts occurs in cholesterol-rich membrane domains and is required or RhoA activation and myogenesis. *The Journal of biological chemistry* **2009,** *284* (34), 23137-45.
52. Barcelona-Estaje, E.; Dalby, M. J.; Cantini, M.; Salmeron-Sanchez, M., You Talking to Me? Cadherin and Integrin Crosstalk in Biomaterial Design. *Advanced healthcare materials* **2021,** *10* (6), e2002048.
53. Kourtidis, A.; Ngok, S. P.; Anastasiadis, P. Z., p120 catenin: an essential regulator o cadherin stability, adhesion-induced signaling, and cancer progression. *Progress in molecular biology and translational science* **2013,** *116*, 409-32.
54. Pal, M.; Bhattacharya, S.; Kalyan, G.; Hazra, S., Cadherin profiling or therapeutic interventions in Epithelial Mesenchymal Transition (EMT) and tumorigenesis. *Experimental cell research* **2018,** *368* (2), 137-146.
55. Seidel, B.; Braeg, S.; Adler, G.; Wedlich, D.; Menke, A., E- and N-cadherin differ with respect to their associated p120ctn iso orms and their ability to suppress invasive growth in pancreatic cancer cells. *Oncogene* **2004,** *23* (32), 5532-42.
56. Anastasiadis, P. Z.; Moon, S. Y.; Thoreson, M. A.; Mariner, D. J.; Craw ord, H. C.; Zheng, Y.; Reynolds, A. B., Inhibition o RhoA by p120 catenin. *Nature cell biology* **2000,** *2* (9), 637-44.
57. Wu, Y.; Ali, M. R. K.; Dong, B.; Han, T.; Chen, K.; Chen, J.; Tang, Y.; Fang, N.; Wang, F.; El-Sayed, M. A., Gold Nanorod Photothermal Therapy Alters Cell Junctions and Actin Network in Inhibiting Cancer Cell Collective Migration. *ACS Nano* **2018,** *12* (9), 9279-9290.
58. Duncan, R. F.; Hershey, J. W., Protein synthesis and protein phosphorylation during heat stress, recovery, and adaptation. *Journal of Cell Biology* **1989,** *109* (4), 1467-1481.
59. Liu, J.; Kang, L.; Ratnayake, I.; Ahrenkiel, P.; Smith, S.; Wang, C., Targeting cancer cell adhesion molecule, CD146, with low-dose gold nanorods and mild hyperthermia disrupts actin cytoskeleton and cancer cell migration. *Journal of Colloid and Interface Science* **2021,** *601*, 556-569.
60. Liu, J.; Kang, L.; Smith, S.; Wang, C., Transmembrane MUC18 Targeted Polydopamine Nanoparticles and a Mild Photothermal Effect Synergistically Disrupt Actin Cytoskeleton and Migration o Cancer Cells. *Nano Letters* **2021,** *21* (22), 9609-9618.

TOC

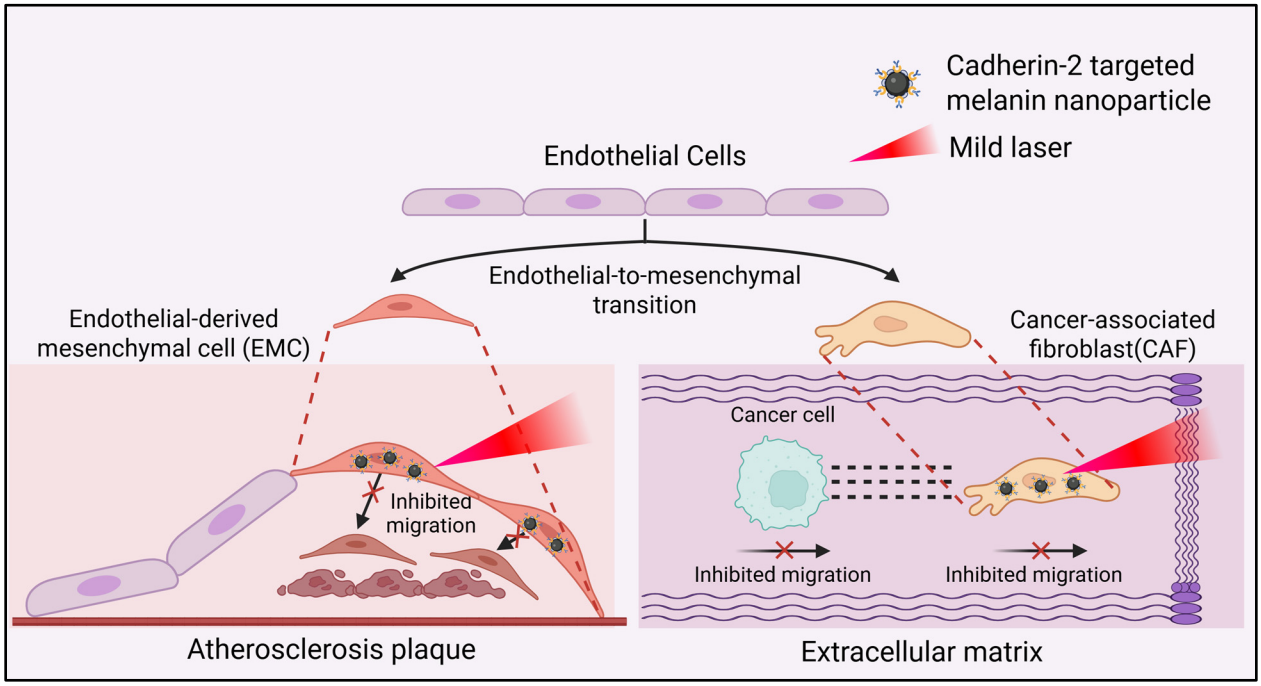
Cadherin-2 targeted
melanin nanoparticle
Mild laser
Endothelial Cells
Endothelial-to-mesenchymal
transition
Endothelial-derived
mesenchymal cell (EMC)
Cancer-associated
fibroblast(CAF)
Inhibited
migration
Cancer cell
Inhibited migration
Inhibited migration
Atherosclerosis plaque
Extracellular matrix